BIOPHYSICS

Structure and mechanism of the osmoregulated choline transporter BetT

Tianjiao Yang[1,2]†, Yuwei Nian[1]†, Huajian Lin[1]†, Jing Li[3]†, Xiang Lin[4], Tianming Li[1], Ruiying Wang[1], Longfei Wang[3], Gwyn A. Beattie[5]*, Jinru Zhang[4]*, Minrui Fan[1,6]*

The choline–glycine betaine pathway plays an important role in bacterial survival in hyperosmotic environments. Osmotic activation of the choline transporter BetT promotes the uptake of external choline for synthesizing the osmoprotective glycine betaine. Here, we report the cryo–electron microscopy structures of *Pseudomonas syringae* BetT in the apo and choline-bound states. Our structure shows that BetT forms a domain-swapped trimer with the C-terminal domain (CTD) of one protomer interacting with the transmembrane domain (TMD) of a neighboring protomer. The substrate choline is bound within a tryptophan prism at the central part of TMD. Together with functional characterization, our results suggest that in *Pseudomonas* species, including the plant pathogen *P. syringae* and the human pathogen *Pseudomonas aeruginosa*, BetT is locked at a low-activity state through CTD-mediated autoinhibition in the absence of osmotic stress, and its hyperosmotic activation involves the release of this autoinhibition.

INTRODUCTION

Coping with water stress is faced by all living organisms (*1*, *2*). Under hypoosmotic conditions, water will flow into the cell, leading to cellular swelling and bursting; while under hyperosmotic conditions (such as high salinity), water will flow out of the cell, resulting in cellular dehydration. Both are detrimental to cellular physiology. Besides, in organisms containing cell walls, water influx or efflux can also cause changes in turgor pressure and affect cell growth (*3*, *4*). To survive in diverse environments of different osmolality, the organisms must respond to water stress and maintain osmotic homeostasis. One conserved strategy ubiquitous in living systems for adapting to hyperosmotic environments is to amass organic osmolytes, also called compatible solutes, which can help adjust osmotic potential without impairing normal cellular activities when present at high concentration (*1*, *5*–*8*). The compatible solutes are mainly composed of three kinds of small molecules: carbohydrates, such as trehalose and inositol; amino acids and derivatives, such as proline and ectoine; and methylammonium and methylsulfonium compounds, such as glycine betaine and dimethylsulfoniopropionate (*5*, *8*, *9*).

Responding to osmotic stress is more critical for the survival of bacteria, which are directly exposed to external environments, than for multicellular organisms, which have protective skins (*10*). In most bacteria, glycine betaine is the preferred compatible solute for osmoprotection (*11*, *12*). As one of the most potent osmoprotectants (*12*, *13*), besides maintaining osmotic balance, glycine betaine can also stabilize proteins in stressed bacterial cells (*14*–*16*). There are two common ways of acquiring glycine betaine: uptake from external environments through transport systems (*7*, *9*, *12*) and synthesis from the precursor choline through the choline–glycine betaine pathway, in which choline is taken up through transporters and then converted to glycine betaine via a two-step enzymatic oxidation reaction (*17*–*19*). Choline is abundant primarily in the form of choline-containing lipids and can be released to the environments through bacterial phospholipases (*20*, *21*), and diverse bacterial species widely harness the choline–to–glycine betaine synthesis pathway for osmoadaptation (*9*, *22*). Notably, the choline–glycine betaine pathway also exists in plants and animals and plays important roles in their responses to salt stress (*8*, *23*, *24*). In the choline–glycine betaine pathway of *Escherichia coli*, choline uptake is mainly mediated by the transporter BetT, and its expression and transport activity are both up-regulated by hyperosmotic stress (*25*). BetT homologs are distributed in many other bacteria, including human pathogens such as *Pseudomonas aeruginosa* and *Acinetobacter baumannii*, and play important roles not only in osmoprotection but also in choline catabolism (*20*, *26*–*33*). It has been shown that BetT is critical for the fitness of the plant pathogen *Pseudomonas syringae* during leaf colonization (*34*), and BetT-mediated choline uptake has also been implicated in contributing to the survival of two major nosocomial pathogens *P. aeruginosa* and *A. baumannii* in human hosts (*20*, *29*, *31*, *35*, *36*). Moreover, BetT has been associated with bacterial thermoprotection and cold adaption (*37*–*39*).

BetT is the founding member of the betaine/carnitine/choline transporter (BCCT) family (*40*), whose members mediate the uptake of compatible solutes for osmoprotection or catabolism in bacteria (*7*, *20*, *41*, *42*). BCCT family members commonly transport substrates containing methylammonium or methylsulfonium groups, but they have different substrate specificities, transport mechanisms, and activity regulation mechanisms. BCCT transporters can be classified into three types: (i) sodium-coupled symporters, such as the betaine transporter BetP; (ii) proton-coupled symporters, such as BetT; and (iii) substrate/product antiporters, such as the L-carnitine/γ-butyrobetaine transporter CaiT (*41*). The three types of BCCT transporters share low sequence identities (<30%). Among them, BetP and BetT are osmoregulated, and their transport activities increase substantially upon high osmolarity stress (*19*, *43*, *44*).

[1]CAS Center for Excellence in Molecular Plant Sciences, Institute of Plant Physiology and Ecology, Chinese Academy of Sciences, Shanghai 200032, China. [2]University of Chinese Academy of Sciences, Beijing 101408, China. [3]School of Pharmaceutical Sciences, Wuhan University, Wuhan 430071, China. [4]State Key Laboratory of Genetic Engineering, Collaborative Innovation Center of Genetics and Development, Department of Biochemistry and Biophysics, School of Life Sciences, Fudan University, Shanghai 200438, China. [5]Department of Plant Pathology, Entomology and Microbiology, Iowa State University, Ames, IA 50011, USA. [6]Key Laboratory of Plant Carbon Capture, Chinese Academy of Sciences, Shanghai 200032, China.
*Corresponding author. Email: gbeattie@iastate.edu (G.A.B.); zhangjr@fudan.edu.cn (J.Z.); mrfan@cemps.ac.cn (M.F.)
†These authors contributed equally to this work.

However, the mechanisms underlying BetT and BetP osmoregulation are likely different because they have completely distinct C-terminal regulatory domains (*28*, *43*). Recent structural studies on BetP and CaiT have provided important insights into the overall architecture of BCCT family transporters and their respective transport mechanisms (*45*–*50*), but the molecular mechanism underlying choline transport of BetT is unknown, and the activity regulation mechanisms of the osmoregulated BCCT transporters are still poorly understood.

To shed light on how BetT recognizes and transports choline, we determined the cryo–electron microscopy (cryo-EM) structures of *P. syringae* BetT in both apo and substrate-bound states. Our structural and functional studies reveal a unique domain-swapped trimer structure of BetT and suggest a C-terminal domain (CTD) autoinhibition-mediated osmoregulation mechanism.

RESULTS

Overall structure

Our biochemical characterization showed that BetT from *P. syringae* pv. tomato DC3000 (PsBetT) was well-behaved on a size exclusion column (fig. S1, A and B). The expression of PsBetT in the choline transporter-deficient *E. coli* strain MKH13 (*51*) in the presence and absence of NaCl, KCl, or sorbitol showed the hyperosmotic activation of choline transport based on a fluorescence assay for endogenous choline (fig. S1C; see Materials and Methods), consistent with previous studies (*19*, *28*). Using cryo-EM, we determined the structures of PsBetT alone and in the presence of choline at 2.57- and 2.59-Å resolutions, respectively (figs. S2 and S3). The high-resolution cryo-EM density maps allowed us to build a complete model for BetT containing both the transmembrane domain (TMD) and CTD (Fig. 1 and fig. S4). Both the apo and choline-bound PsBetT structures are captured in the occluded state.

In both structures, PsBetT is a trimer (Fig. 1, A and B), consistent with the typical trimeric state of the BCCT family transporters (*41*, *45*, *48*, *49*). Each PsBetT protomer is composed of the transport unit TMD (residues 11 to 515) and the regulatory domain CTD (residues 528 to 664) in the cytosol (Fig. 1C and fig. S5A) (*43*). The TMD consists of 12 transmembrane helices (TM1 to TM12) and adopts an amino acid–polyamine-organocation (APC) superfamily fold with TM3–7 and TM8–12 forming inverted repeats (Fig. 1D). Between TM7 and TM8, there is a curved amphiphilic helix (H2) parallel to the membrane on the periplasmic side. The CTD of PsBetT (137 residues) is much larger than that of BetP, which is composed of a long α helix consisting of 49 residues (*45*). The CTD shows a mixed α/β structure composed of three α helices (α1 to α3) and five β strands (β1 to β5) (Fig. 1E). Dali server analysis showed that the fold of the CTD of PsBetT is similar to that of the frataxin protein family despite the low sequence similarity (<10%) of these proteins (fig. S5B). The CTD is connected to the TMD through a flexible linker consisting of 12 residues. Notably, in the PsBetT trimer, the CTD of one protomer is under the TMD of a neighboring protomer, yielding a domain-swapped configuration (Fig. 1B), as identified previously in BetP (*45*).

Choline-binding site

In the presence of choline, we observed a strong thumbtack-like nonprotein density in each protomer of the PsBetT trimer (Fig. 2A), at a location corresponding to the betaine-binding site of BetP and the primary substrate-binding site of CaiT (*45*, *46*, *48*, *49*). These densities were assigned as choline because they are absent in the apo PsBetT structure. Choline binds near the unwound region of TM3 halfway through the membrane and is occluded from both the periplasmic and cytosolic sides (Fig. 2B). On one side, the positively charged methylammonium moiety of choline forms cation-π interactions with three tryptophan residues of TM8, W327, W328, and W331, which have a configuration of a tryptophan prism (Fig. 2C). Notably, in the apo state, the arrangement of the three tryptophan residues in PsBetT is not favorable for choline binding, and two of them (W327 and W328) show side-chain rotamer changes in the choline-bound state (Fig. 2D). On the other side, the hydroxyl group of choline forms a hydrogen bond with the main-chain oxygen of G105 at the unwound part of TM3 (Fig. 2C). These choline-interacting residues are highly conserved among BetT of different species (fig. S6). Overall, the binding mode of choline in PsBetT is similar to that in the choline-binding protein ChoX and choline transporter LicB (*52*, *53*), and it also shows similarity to the binding mode of betaine in the betaine-binding protein OpuAC and betaine transporter BetP (*46*, *54*). To probe the choline-binding site of PsBetT, we performed functional characterizations on mutants with the choline-interacting tryptophan residues replaced by residues lacking an indole ring. Substitution of W327 or W328 with leucine or alanine substantially impaired choline transport activity (Fig. 2E and fig. S7A). These results support our structural observations on choline binding.

Proton-binding site

To probe the proton dependence of PsBetT, we analyzed its choline transport activity by using the protonophores carbonyl cyanide *m*-chlorophenylhydrazone (CCCP) and carbonyl cyanide 4-(trifluoromethoxy)phenylhydrazone (FCCP). Our results showed that CCCP or FCCP can abolish the choline transport activity of PsBetT (fig. S7C), supporting its proton coupling, consistent with previous studies on *E. coli* BetT (EcBetT) (*19*). To identify the proton-binding site of PsBetT, we mutated all the potential protonatable residues in the TMD individually and characterized their choline transport activities. Our results showed that among the 24 alanine substitution mutants, only two (D210A and E403A) substantially impaired the choline transport (fig. S7D). Furthermore, we characterized the mutants with D210 and E403 substituted with non-protonatable hydrophilic residues. Our results showed that the D210N and D210T mutations substantially impaired the choline transport, similar to the D210A mutant (Fig. 3A and fig. S7E). However, the E403Q mutant behaved similarly to wild-type (WT) PsBetT but not the E403A mutant (fig. S7D), indicating that E403A may affect protein folding/structure. Therefore, our functional studies suggested that D210 contributes to proton coupling in PsBetT. Consistently, our structure showed that D210 is actually located near the choline-binding site in the substrate transport pathway. D210 of TM5 forms hydrogen bond interactions with S107 and T109 of TM3 (Fig. 3B). Therefore, it is probable that protonation/deprotonation of D210 may affect interhelical interactions and local conformational change and choline transport. Notably, D210 is fully conserved in BetT homologs of *Pseudomonas* species but variable in BetT of *E. coli* and other species (fig. S6). Consistent with the sequence difference, another acidic residue (D108) from TM3 has been suggested to be the proton-binding site of EcBetT (*55*). In PsBetT, the residue T109 that occupies the equivalent position of this D108 of EcBetT interacts with D210.

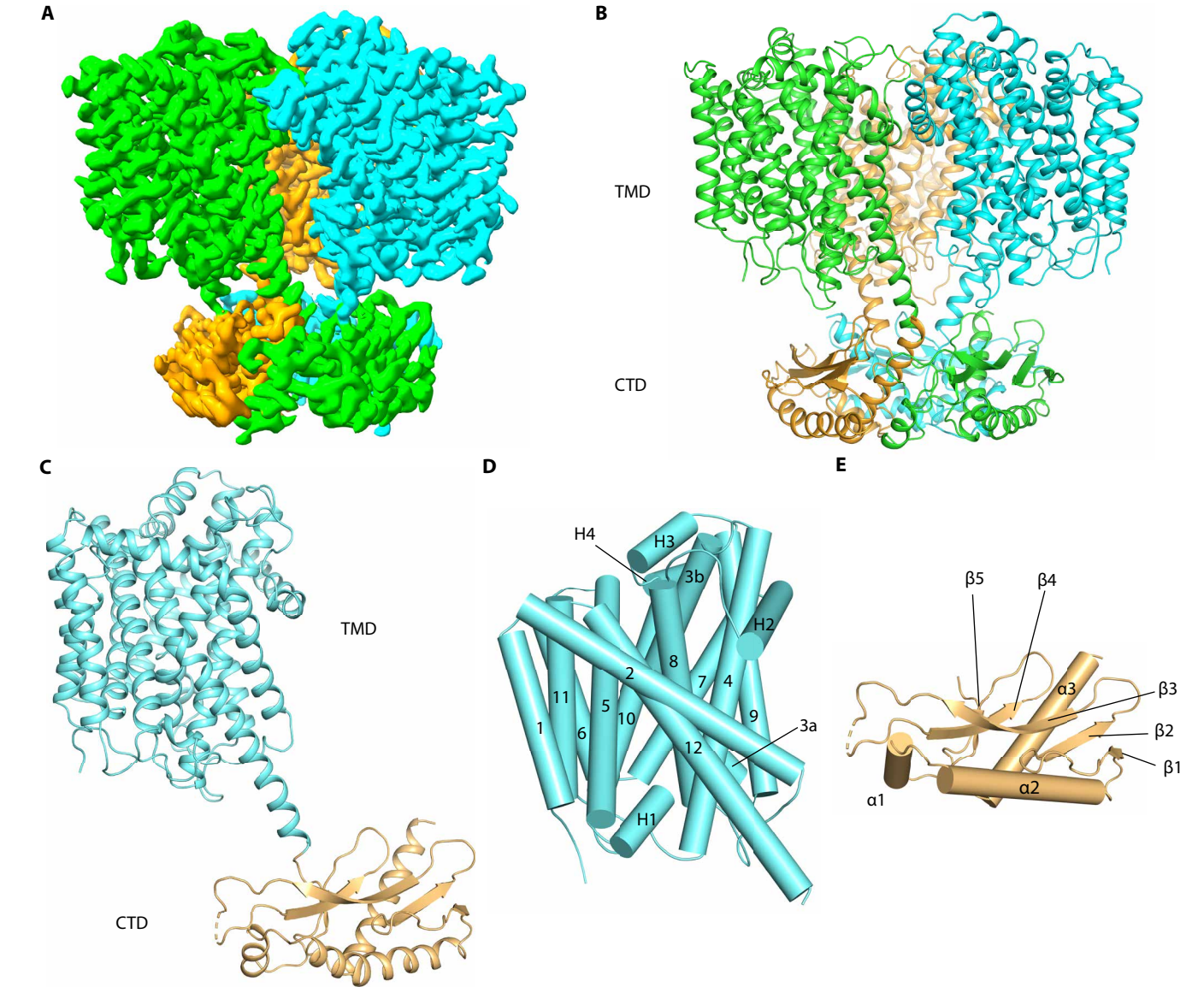

Fig. 1. Structure of PsBetT. (**A**) Cryo-EM density map of PsBetT. (**B**) Overall structure of PsBetT. The three protomers are colored green, cyan, and orange, respectively. (**C**) Structure of PsBetT monomer. The TMD and CTD are colored cyan and wheat, respectively. (**D**) TMD structure of one PsBetT subunit. (**E**) CTD structure of one PsBetT subunit.

Trimer organization

In the trimeric PsBetT structure, both the TMD and the cytosolic CTD are organized as a trimer (Fig. 1, A and B). In the TMD, trimer formation is mainly mediated by helix H2, which makes contacts with H2′, the loop between H2′ and TM8′, and TM2′ of the neighboring protomer on the periplasmic side (fig. S8A). Below H2, there are large clefts between neighboring protomers which are filled with extra densities, potentially lipid molecules (fig. S8, A and B). In the soluble cytosolic part, cross-protomer interactions mainly involve hydrophobic interactions and salt bridges between helices α2 and α3 of one CTD and helix α1′ and the loop between strands β3′ and β4′ of a neighboring CTD; moreover, the trimer interface exhibits a good shape complementarity (fig. S8C). To assess the role of the CTD in the trimer formation of PsBetT, we deleted the CTD (hereafter named $PsBetT_{\Delta CTD}$) and performed cross-linking. Our result showed that $PsBetT_{\Delta CTD}$ still primarily forms trimers (fig. S8D), indicating that the CTD is dispensable for PsBetT trimer formation. This is consistent with the ability of CaiT (intrinsically lacking a CTD) and CTD-deleted BetP to form stable trimers (*48*, *49*, *56*).

CTD-mediated osmoregulation

To explore whether the CTD is involved in the osmotic activation of PsBetT, we characterized the choline transport activity of $PsBetT_{\Delta CTD}$ under low and high osmolarity conditions using NaCl as an osmolyte. We found that the transport activity of $PsBetT_{\Delta CTD}$ under low-salt conditions is comparable to that of WT PsBetT under high-salt conditions; that is, removal of the CTD enabled PsBetT to be highly active in the absence of hyperosmotic stress (Fig. 4A). Our finding

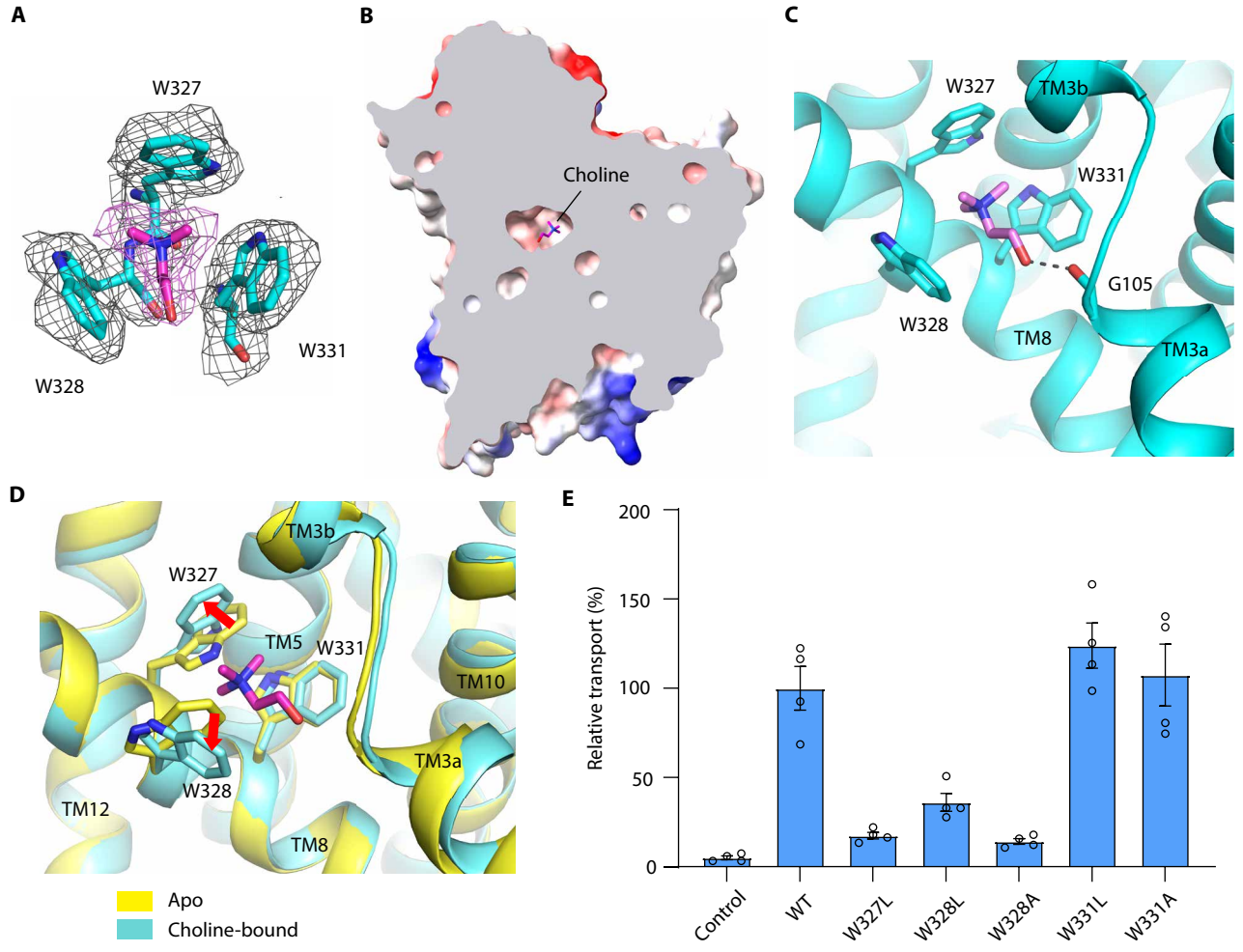

Fig. 2. The choline-binding site of PsBetT. (**A**) Cryo-EM densities of choline and surrounding tryptophan residues. The choline molecule and the tryptophan residues are shown as magenta and cyan sticks, respectively. (**B**) Sliced view of PsBetT in the choline-bound state. (**C**) Interactions between choline and PsBetT. The hydrogen bond is shown as a dashed line. (**D**) Local side-chain rotamer changes between apo (yellow) and choline-bound (cyan) PsBetT. (**E**) Choline transport activities of PsBetT variants with mutations at the choline-binding site [normalized to the wild type (WT); means ± SEM, $n = 4$ independent experiments].

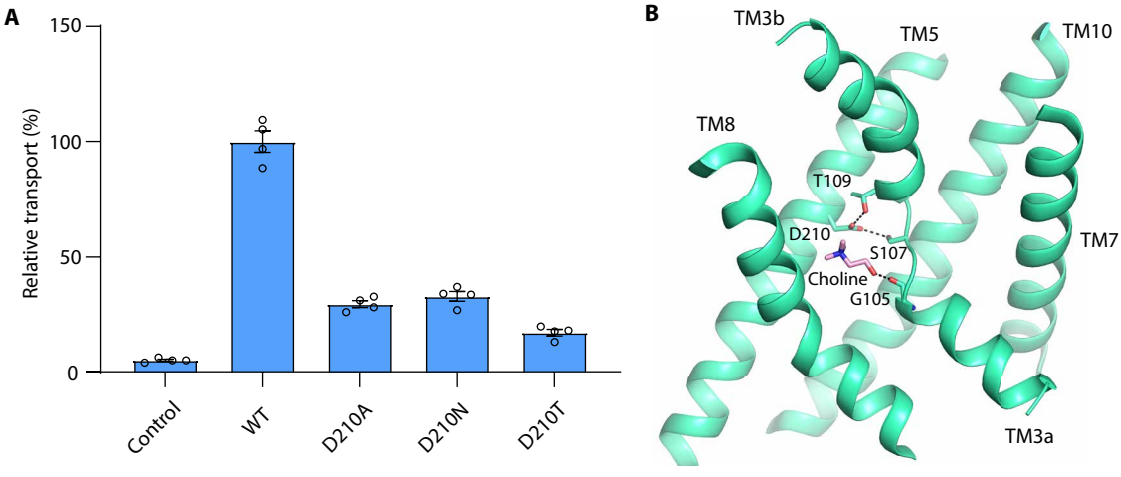

Fig. 3. The proton-binding site of PsBetT. (**A**) Choline transport activities of PsBetT variants with mutations at the potential proton-binding site (normalized to WT; means ± SEM, $n = 4$ independent experiments). (**B**) The surrounding environment of the proposed proton-binding site D210.

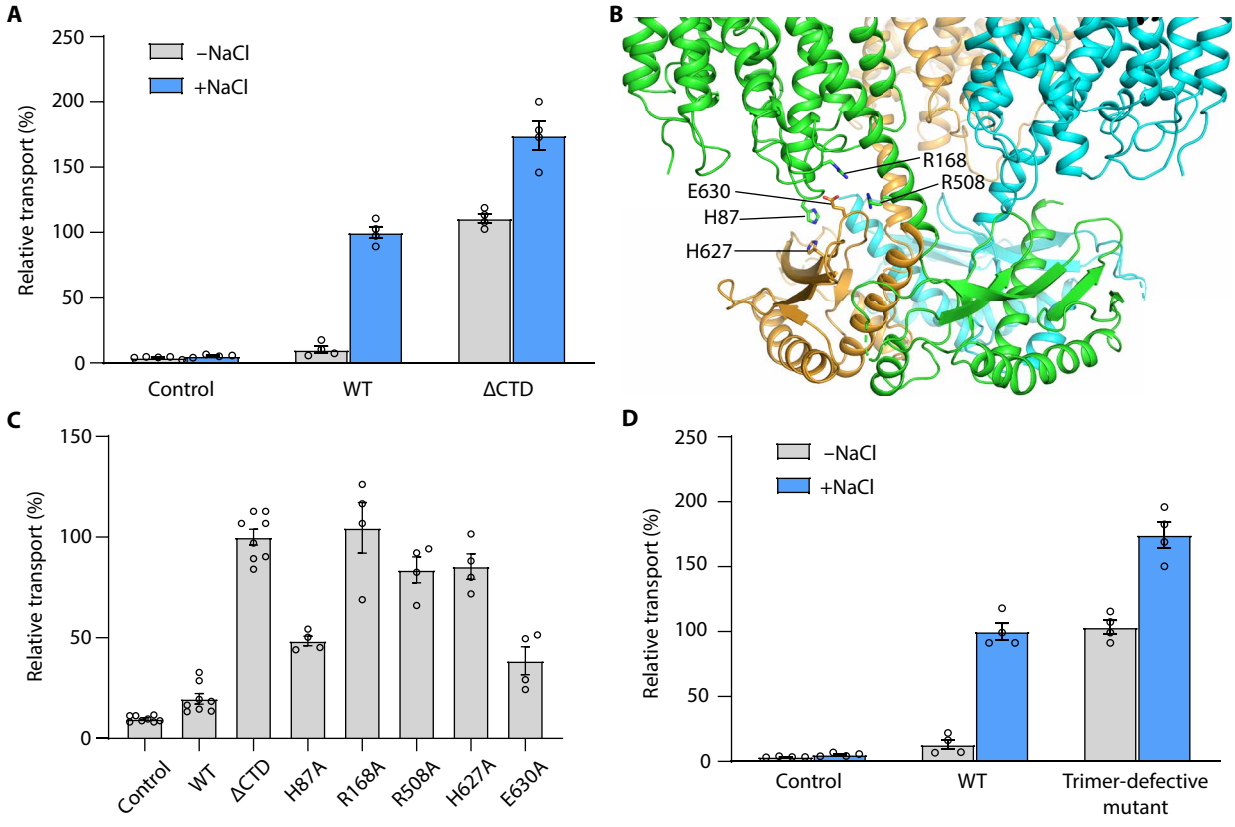

Fig. 4. CTD autoinhibition of PsBetT. (**A**) Choline transport activities of PsBetT WT and ΔCTD under low and high osmolarity conditions (normalized to WT; means ± SEM, $n = 4$ independent experiments). NaCl (0.5 M) was added to introduce high osmolarity. (**B**) CTD-TMD interaction interface. The key residues at the interface are shown as sticks. (**C**) Choline transport activities of PsBetT variants with mutations at the CTD-TMD interface under low osmolarity conditions (normalized to ΔCTD; means ± SEM, $n = 4$ independent experiments, except for WT, ΔCTD, and control, which are $n = 8$ independent experiments). (**D**) Choline transport activities of PsBetT WT and trimer-defective mutant (W57A, F305A, and Y310A) under low and high osmolarity conditions (normalized to WT; means ± SEM, $n = 4$ independent experiments). BetT-mediated choline uptake was not saturated after 1 hour.

indicates that the CTD maintains PsBetT in a low-activity state under non-hyperosmotic conditions, thus illustrating an autoinhibitory role in PsBetT osmoregulation.

How does the CTD autoinhibit PsBetT's activity? Our structural analysis provides a hint, namely, that contact between the CTD of one protomer and the intraprotomeric loop between TM2′ and TM3′ of the neighboring protomer (Figs. 1D and 4B) might restrict a conformational change of this loop and associated outward movement of TM3a; the latter is presumably required for the release of a substrate into the cytosol as observed in BetP (*46*). Our structure shows that two kinds of interactions contribute to the positioning of the $CTD^{protomer\ A}$ and $TMD^{protomer\ B}$ in the PsBetT trimer: one is the interaction between H627 of $CTD^{protomer\ A}$ and H87 of $TMD^{protomer\ B}$ and the other is the electrostatic interactions between E630 of $CTD^{protomer\ A}$ and R168 and R508 of $TMD^{protomer\ B}$ (Fig. 4B). Notably, our cryo-EM map suggests that H87, H627, and D634 may coordinate a metal ion at the CTD-TMD contact site and an unidentified carboxyl group–containing small molecule might also contribute to the ion coordination (fig. S8E). To probe the CTD-TMD interactions in the osmoregulation of PsBetT, we characterized the effects of interfacial mutations on its choline transport activity. We found that substitution of the abovementioned CTD-TMD interfacial residues with alanine all increased PsBetT's activity under low-salt conditions (Fig. 4C). These results are consistent with our prediction that PsBetT is autoinhibited by the CTD.

Because the autoinhibition of PsBetT at low osmolarity involves intersubunit CTD-TMD interactions, our model predicts that trimer formation is critical for PsBetT osmoregulation. On the basis of previous studies with the BetP trimer (*57*), we designed several PsBetT mutants with key interfacial residues substituted with alanine and assessed their trimer formation using size exclusion chromatography. We found that pyramiding the W57A, F305A, and Y310A mutations disrupted PsBetT trimer formation (fig. S7B), and this triple mutant exhibited high choline transport activity under low-salt conditions (Fig. 4D), consistent with our model of PsBetT autoinhibition at low osmolarity. Osmoregulation of BetP also requires the formation of intact trimers (*57*). These results suggest that trimer formation is a common strategy harnessed for osmoregulation by osmosensing BCCT transporters.

We noticed that the residues mediating CTD-TMD interactions in PsBetT are fully conserved among BetT homologs of *Pseudomonas* species, including the human pathogen *P. aeruginosa*, but are variable in other bacterial species, such as *E. coli*. To explore whether the CTD autoinhibition mechanism is harnessed for the osmoregulation of BetT in other bacteria, we deleted the CTDs of the BetT of *P. aeruginosa* (PaBetT) and *E. coli* and characterized their choline

transport activities. Removing the CTD of PaBetT made it active in the absence of hyperosmotic stress, similar to PsBetT (fig. S9A). In contrast, deleting the CTD of EcBetT did not increase its transport activity under low osmolarity but did make it unable to be fully activated by high osmolarity (fig. S9B). This indicates that the CTD plays different roles in BetT osmoregulation among bacterial species. In species with BetT that share high homology with PsBetT, the osmoregulation of BetT likely involves CTD-mediated autoinhibition at low osmolarity. In contrast, in species with BetT that is similar to EcBetT, the CTD likely contributes to hyperosmotic activation.

DISCUSSION

In summary, we have determined the structure of bacterial osmoregulated choline transporter BetT, identified its substrate-binding site, and completed our knowledge about the BCCT family transporters. Our results suggest that osmoregulation of BetT activity is achieved by its CTD-mediated autoinhibition and hyperosmotic stress-triggered release of this inhibition in *Pseudomonas* species. Autoinhibition has been found in the activity regulation of many transporters, and it typically involves the interaction of a soluble part with TMD that leads to either blocking of the substrate translocation pathway or obstruction of conformational changes of TMD (*58*–*62*). In PsBetT, it is likely that CTD-TMD interactions restrict the conformational changes of TMD that are required for substrate release. Further studies will be required to elucidate how the osmotic stress sensed by BetT induces changes in CTD-TMD organization and choline transport.

MATERIALS AND METHODS

Protein expression and purification

The coding sequence of BetT from *P. syringae* pv. tomato DC3000 with a C-terminal Strep-tag was cloned into the pETDuet-1 vector. The plasmid was then transformed into *E. coli* strain Rosetta (DE3) and the cells were grown overnight at 37°C. After inoculating with a ratio of 1:100, the cells were grown at 37°C until the OD_{600} (optical density at 600 nm) reached 0.6 to 0.8. Then, 0.2 mM isopropyl-β-D-thiogalactopyranoside (IPTG) was added to induce protein expression. After culturing at 18°C for 16 hours, the cells were harvested and stored at −80°C.

To purify PsBetT, the cells were resuspended in buffer A [50 mM tris (pH 7.4), 150 mM NaCl, and 0.5 mM phenylmethylsulfonyl fluoride (PMSF)] and lysed using an ultrasonic cell disruptor. Then, the membrane proteins were extracted using 1.5% lauryl maltose neopentyl glycol (LMNG; Anatrace)/0.2% cholesteryl hemisuccinate (CHS; Anatrace) at 4°C for 2 hours. After centrifuging at 17,000 rpm for 1 hour, the supernatant was incubated with prewashed Streptactin Beads 4FF (Smart-Lifesciences) at 4°C for 2 hours. The slurry was poured into a gravity column, and the resin was extensively washed with buffer B [20 mM tris (pH 7.4), 150 mM NaCl, and 0.05% glyco-diosgenin (GDN)]. PsBetT was eluted with buffer C [20 mM tris (pH 7.4), 150 mM NaCl, and 0.01% GDN] supplemented with 10 mM dethiobiotin. The protein was further polished through gel filtration using a Superose 6 increase column (Cytiva).

To purify PsBetT bound with choline, the cells were resuspended in buffer D [50 mM MES (pH 6.0), 100 mM NaCl, 50 mM choline chloride, and 0.5 mM PMSF] and lysed using an ultrasonic cell disruptor. Then, the membrane proteins were extracted using 1.5% LMNG/CHS at 4°C for 2 hours. After centrifugating at 17,000 rpm for 1 hour, the supernatant was incubated with pre-washed Streptactin Beads 4FF at 4°C for 2 hours. The slurry was poured into a gravity column, and the resin was extensively washed with buffer E [20 mM MES (pH 6.0), 100 mM NaCl, 50 mM choline chloride, and 0.05% GDN]. PsBetT was eluted with buffer F [20 mM MES (pH 6.0), 100 mM NaCl, 50 mM choline chloride, and 0.01% GDN] supplemented with 10 mM dethiobiotin. The protein was further polished through gel filtration using a Superose 6 increase column. Both samples were concentrated to 7 mg/ml for cryo-EM grid preparation.

Cryo-EM sample preparation and data collection

Grids (300 mesh, R2/1; Quantifoil, Germany) were glow-discharged by a PELCO easiGlow machine (15 mA, 1 min). The purified protein (3.5 μl) was applied to the grid and incubated for 20 s (8°C, 100% humidity), and then the grid was blotted with filter paper for 5 s and plunge-frozen in liquid ethane cooled by liquid nitrogen by a vitrobot (Vitrobot Mark IV, Thermo Fisher Scientific). Samples were imaged with a 200-kV electron microscope (Talos Arctica, Thermo Fisher Scientific), and grids generating images with good contrast and particle distribution were further imaged using a 300-kV electron microscope (Titan Krios G4, Thermo Fisher Scientific) equipped with a Gatan K3 direct electron detector. Data collection was performed in super-resolution counting mode at a magnification of approximately ×105,000, corresponding to a physical pixel size of 0.86 Å. Movies were recorded with a total exposure of 50 electrons/$Å^2$, and the defocus range was set from −1.5 to −2.5 μm. The data collection statistics are summarized in table S1.

Cryo-EM data processing

Cryo-EM datasets collected from apo and choline-bound BetT were processed and analyzed using similar procedures, and all image processing steps were performed in cryoSPARC (v4.1.2) (*63*) or RELION (v4.0.1) (*64*). Movies acquired with K3 detectors were subjected to MotionCor2 (*65*) and patch motion correction for beam-induced drift, respectively. Then, the contrast transfer function (CTF) parameters of micrographs were estimated by Gctf (*66*) and patch CTF, respectively. Particles were picked by a manual picker and a template picker within cryoSPARC or autopicking in RELION. After two to four rounds of two-dimensional (2D) classification in cryoSPARC, the remaining particles that yielded clear secondary structural features were selected for ab initio 3D model generation (six classes; C3 symmetry was applied during all subsequent 3D reconstruction). The particles were then subjected to hetero-refinement with the input of six volumes generated ab initio as the references. Particles belonging to the class that generated a cryo-EM map with sufficient resolution were subjected to nonuniform refinement and local refinement, which resulted in maps of 2.95- and 2.59-Å resolutions for apo and choline-bound PsBetT, respectively. For the dataset of apo PsBetT, further 3D classification was carried out to improve the local resolution of the CTD. Last, the particles belonging to classes that exhibited high-quality CTD density were resubjected to nonuniform refinement, which resulted in a map with a resolution of 2.96 Å. To further improve the overall resolution, the cryoSPARC-refined particles were exported into RELION for Bayesian polishing (*67*). Last, nonuniform refinement was performed, resulting in the highest

resolution of 2.57 Å. The image processing workflows are summarized in figs. S2 and S3.

Model building and refinement

Cryo-EM maps generated in cryoSPARC 3D refinements, either further sharpened with B-factor sharpening or postprocessed in DeepEMhancer (*68*), were used for model building and figure preparation. A structural model predicted by AlphaFold (*69*) was selected as the initial template. After manual adjustments of local parts in COOT (*70*), the models were further refined by real-space refinement in PHENIX (*71*). The geometry of refined models was validated by MolProbity (*72*). All structural figures were prepared in PyMOL (*73*) and UCSF Chimera (*74*) or Chimera X (*75*).

Cell-based choline uptake assay

The coding sequences of PsBetT and mutant derivatives were cloned into the pBAD vector. *E. coli* strain MKH13 cells were transformed with the plasmids and grown overnight at 37°C. After inoculating with a ratio of 1:100 into 3 ml of fresh LB medium containing ampicillin (100 μg/ml), the cells were grown at 37°C until the OD_{600} reached 0.7 to 0.8. Protein expression was induced with 0.02% arabinose for 4 hours. The cells were harvested, washed once with M63 medium, and resuspended in M63 medium to an OD_{600} of 1.0. Three milliliters of the cells was used for the choline uptake assay. Chloramphenicol (100 μg/ml) was added to the cells to terminate protein expression (*18*). After incubating at 37°C for 5 min, 15 mM choline chloride and 0.5 M NaCl (or 0.5 M KCl or 0.8 M sorbitol) were added, and the cells were incubated at 37°C for 1 hour with shaking. The cells were harvested and washed four times with ice-cold 1 M NaCl. Then, cells were resuspended in the buffer containing 50 mM tris (pH 7.4) and 150 mM NaCl and lysed with glass beads using a mixer mill. The lysate was spun at 13,200 rpm for 1 min, and the choline in the supernatant was detected with the Amplite Choline Quantitation Kit (AAT Bioquest) according to the manufacturer's instructions. Briefly, 50 μl of supernatant was mixed with 50 μl of work solution from the kit, and the mixture was incubated at 37°C for 20 min. Then, the result was read with a fluorescence microplate reader at Ex/Em (excitation/emission) = 540/590 nm. In this experimental setting, choline was detected with Amplite Red through the choline oxidase and hydrogen peroxide–mediated enzyme coupling reactions, and the fluorescence intensity of Amplite Red was proportional to the concentration of choline.

Western blot

The coding sequences of BetT WT and choline-binding site mutants with a C-terminal Strep-tag were cloned into the pBAD vector. *E. coli* strain MKH13 cells were transformed with the plasmids and grown overnight at 37°C. After inoculating with a ratio of 1:100 into 3 ml of fresh LB medium containing ampicillin (100 μg/ml), the cells were grown at 37°C until the OD_{600} reached 0.7 to 0.8. Protein expression was induced with 0.02% arabinose for 4 hours. The cells were harvested and washed once with the buffer containing 20 mM tris (pH 7.4) and 150 mM NaCl. The cell pellet was resuspended and the OD_{600} was brought to 1.0. Three milliliters of the cells was spun down and resuspended in 100 μl of buffer. Five microliters of the cells was lysed by adding SDS–polyacrylamide gel electrophoresis (SDS-PAGE) loading buffer, and the total proteins were separated by SDS-PAGE, electroblotted to a poly(vinylidene fluoride) membrane (Millipore) and probed using mouse anti-Strep antibody (ABclonal).

Cross-linking

$PsBetT_{\Delta CTD}$ (residues 516 to 664 were deleted) was expressed and purified as described above for full-length PsBetT. For cross-linking, 10 μl of the protein at 0.33 mg/ml was treated with 0.13% glutaraldehyde in a buffer containing 20 mM Hepes (pH 7.4), 150 mM NaCl, and 0.01% GDN at 20°C for different durations (5, 10, 30, 60, and 120 min). The reaction was terminated by the addition of 1 μl of 1 M tris (pH 7.4), and the reaction products were mixed with SDS-PAGE loading buffer and analyzed by SDS-PAGE.

Fluorescence detection size exclusion chromatography

The coding sequences of the WT PsBetT and trimer-interface mutant derivatives that were fused with C-terminal green fluorescent protein (GFP) were cloned into the pETDuet-1 vector. The plasmids were then transformed into *E. coli* strain Rosetta (DE3), and the cells were grown overnight at 37°C. After inoculating with a ratio of 1:100 into 3 ml of fresh LB medium containing ampicillin (100 μg/ml) and chloramphenicol (50 μg/ml), the cells were grown at 37°C until the OD_{600} reached 0.6 to 0.8. Then, 0.2 mM IPTG was added to induce protein expression. After culturing at 18°C for 16 hours, the cells were harvested and lysed in the buffer containing 50 mM tris (pH 7.4), 150 mM NaCl, and 0.5 mM PMSF. LMNG (1.5%)/CHS was added to the lysate for membrane protein extraction. After incubating at 4°C for 2 hours, the lysate was spun at 14,500 rpm for 30 min, and the supernatant was loaded onto a Superose 6 increase column pre-equilibrated with the buffer containing 20 mM tris (pH 7.4), 150 mM NaCl, and 0.0034% LMNG/CHS. The samples were detected by a fluorescence detector (Shimadzu; Ex/Em = 480/510 nm for the GFP signal). The flow rate was 0.4 ml/min.

Supplementary Materials

This PDF file includes:

Figs. S1 to S9
Table S1

REFERENCES AND NOTES

1. P. H. Yancey, M. E. Clark, S. C. Hand, R. D. Bowlus, G. N. Somero, Living with water stress: Evolution of osmolyte systems. *Science* **217**, 1214–1222 (1982).
2. J. Danziger, M. L. Zeidel, Osmotic homeostasis. *Clin. J. Am. Soc. Nephrol.* **10**, 852–862 (2015).
3. O. Ali, I. Cheddadi, B. Landrein, Y. Long, Revisiting the relationship between turgor pressure and plant cell growth. *New Phytol.* **238**, 62–69 (2023).
4. E. R. Rojas, K. C. Huang, Regulation of microbial growth by turgor pressure. *Curr. Opin. Microbiol.* **42**, 62–70 (2018).
5. P. H. Yancey, Organic osmolytes as compatible, metabolic and counteracting cytoprotectants in high osmolarity and other stresses. *J. Exp. Biol.* **208**, 2819–2830 (2005).
6. J. M. Wood, Bacterial osmoregulation: A paradigm for the study of cellular homeostasis. *Annu. Rev. Microbiol.* **65**, 215–238 (2011).
7. E. Bremer, R. Kramer, Responses of microorganisms to osmotic stress. *Annu. Rev. Microbiol.* **73**, 313–334 (2019).
8. D. Rhodes, A. D. Hanson, Quaternary ammonium and tertiary sulfonium compounds in higher plants. *Annu. Rev. Plant. Physiol. Plant. Mol. Biol.* **44**, 357–384 (1993).
9. B. Kempf, E. Bremer, Uptake and synthesis of compatible solutes as microbial stress responses to high-osmolality environments. *Arch. Microbiol.* **170**, 319–330 (1998).
10. H. Wennerstrom, M. Oliveberg, On the osmotic pressure of cells. *QRB Discov.* **3**, e12 (2022).
11. L. N. Csonka, A. D. Hanson, Prokaryotic osmoregulation: Genetics and physiology. *Annu. Rev. Microbiol.* **45**, 569–606 (1991).
12. J. M. Wood, E. Bremer, L. N. Csonka, R. Kraemer, B. Poolman, T. van der Heide, L. T. Smith, Osmosensing and osmoregulatory compatible solute accumulation by bacteria. *Comp. Biochem. Physiol. A Mol. Integr. Physiol.* **130**, 437–460 (2001).
13. D. Le Rudulier, A. R. Strom, A. M. Dandekar, L. T. Smith, R. C. Valentine, Molecular biology of osmoregulation. *Science* **224**, 1064–1068 (1984).

14. M. M. Santoro, Y. Liu, S. M. Khan, L. X. Hou, D. W. Bolen, Increased thermal stability of proteins in the presence of naturally occurring osmolytes. *Biochemistry* **31**, 5278–5283 (1992).
15. S. Bourot, O. Sire, A. Trautwetter, T. Touze, L. F. Wu, C. Blanco, T. Bernard, Glycine betaine-assisted protein folding in a *lysA* mutant of *Escherichia coli*. *J. Biol. Chem.* **275**, 1050–1056 (2000).
16. S. S. Stadmiller, A. H. Gorensek-Benitez, A. J. Guseman, G. J. Pielak, Osmotic shock induced protein destabilization in living cells and its reversal by glycine betaine. *J. Mol. Biol.* **429**, 1155–1161 (2017).
17. B. Landfald, A. R. Strom, Choline-glycine betaine pathway confers a high level of osmotic tolerance in *Escherichia coli*. *J. Bacteriol.* **165**, 849–855 (1986).
18. P. A. Andresen, I. Kaasen, O. B. Styrvold, G. Boulnois, A. R. Strøm, Molecular cloning, physical mapping and expression of the *bet* genes governing the osmoregulatory choline-glycine betaine pathway of *Escherichia coli*. *J. Gen. Microbiol.* **134**, 1737–1746 (1988).
19. T. Lamark, I. Kaasen, M. W. Eshoo, P. Falkenberg, J. McDougall, A. R. Strøm, DNA sequence and analysis of the *bet* genes encoding the osmoregulatory choline-glycine betaine pathway of *Escherichia coli*. *Mol. Microbiol.* **5**, 1049–1064 (1991).
20. M. J. Wargo, Homeostasis and catabolism of choline and glycine betaine: Lessons from *Pseudomonas aeruginosa*. *Appl. Environ. Microbiol.* **79**, 2112–2120 (2013).
21. J. Boch, B. Kempf, E. Bremer, Osmoregulation in *Bacillus subtilis*: Synthesis of the osmoprotectant glycine betaine from exogenously provided choline. *J. Bacteriol.* **176**, 5364–5371 (1994).
22. G. J. Gregory, E. F. Boyd, Stressed out: Bacterial response to high salinity using compatible solute biosynthesis and uptake systems, lessons from *Vibrionaceae*. *Comput. Struct. Biotechnol. J.* **19**, 1014–1027 (2021).
23. T. H. H. Chen, N. Murata, Enhancement of tolerance of abiotic stress by metabolic engineering of betaines and other compatible solutes. *Curr. Opin. Plant Biol.* **5**, 250–257 (2002).
24. J. Dragolovich, Dealing with salt stress in animal cells: The role and regulation of glycine betaine concentrations. *J. Exp. Zool.* **268**, 139–144 (1994).
25. A. R. Strøm, Osmoregulation in the model organism *Escherichia coli*: Genes governing the synthesis of glycine betaine and trehalose and their use in metabolic engineering of stress tolerance. *J. Biosci.* **23**, 437–445 (1998).
26. R. Rosenstein, D. Futter-Bryniok, F. Gotz, The choline-converting pathway in *Staphylococcus xylosus* C2A: Genetic and physiological characterization. *J. Bacteriol.* **181**, 2273–2278 (1999).
27. X. Fan, C. D. Pericone, E. Lysenko, H. Goldfine, J. N. Weiser, Multiple mechanisms for choline transport and utilization in *Haemophilus influenzae*. *Mol. Microbiol.* **50**, 537–548 (2003).
28. C. Chen, G. A. Beattie, *Pseudomonas syringae* BetT is a low-affinity choline transporter that is responsible for superior osmoprotection by choline over glycine betaine. *J. Bacteriol.* **190**, 2717–2725 (2008).
29. A. A. Malek, C. Chen, M. J. Wargo, G. A. Beattie, D. A. Hogan, Roles of three transporters, CbcXWV, BetT1, and BetT3, in *Pseudomonas aeruginosa* choline uptake for catabolism. *J. Bacteriol.* **193**, 3033–3041 (2011).
30. M. Sand, J. Stahl, I. Waclawska, C. Ziegler, B. Averhoff, Identification of an osmo-dependent and an osmo-independent choline transporter in *Acinetobacter baylyi*: Implications in osmostress protection and metabolic adaptation. *Environ. Microbiol.* **16**, 1490–1502 (2014).
31. J. Breisch, B. Averhoff, Identification of osmo-dependent and osmo-independent betaine-choline-carnitine transporters in *Acinetobacter baumannii*: Role in osmostress protection and metabolic adaptation. *Environ. Microbiol.* **22**, 2724–2735 (2020).
32. I. Lidbury, G. Kimberley, D. J. Scanlan, J. C. Murrell, Y. Chen, Comparative genomics and mutagenesis analyses of choline metabolism in the marine *Roseobacter* clade. *Environ. Microbiol.* **17**, 5048–5062 (2015).
33. L. M. Westermann, I. Lidbury, C.-Y. Li, N. Wang, A. R. J. Murphy, M. D. M. Aguilo Ferretjans, M. Quareshy, M. Shanmugan, A. Torcello-Requena, E. Silvano, Y. Z. Zhang, C. A. Blindauer, Y. Chen, D. J. Scanlan, Bacterial catabolism of membrane phospholipids links marine biogeochemical cycles. *Sci. Adv.* **9**, eadf5122 (2023).
34. C. Chen, S. Li, D. R. McKeever, G. A. Beattie, The widespread plant-colonizing bacterial species *Pseudomonas syringae* detects and exploits an extracellular pool of choline in hosts. *Plant J.* **75**, 891–902 (2013).
35. M. S. Son, W. J. Matthews Jr., Y. Kang, D. T. Nguyen, T. T. Hoang, In vivo evidence of *Pseudomonas aeruginosa* nutrient acquisition and pathogenesis in the lungs of cystic fibrosis patients. *Infect. Immun.* **75**, 5313–5324 (2007).
36. J. Dingemans, P. Monsieurs, S. H. Yu, A. Crabbe, K. U. Forstner, A. Malfroot, P. Cornelis, R. Van Houdt, Effect of shear stress on *Pseudomonas aeruginosa* isolated from the cystic fibrosis lung. *mBio* **7**, e00813–e00816 (2016).
37. T. Caldas, N. Demont-Caulet, A. Ghazi, G. Richarme, Thermoprotection by glycine betaine and choline. *Microbiology* **145**, 2543–2548 (1999).
38. I. Raymond-Bouchard, J. Tremblay, I. Altshuler, C. W. Greer, L. G. Whyte, Comparative transcriptomics of cold growth and adaptive features of a eury- and steno-psychrophile. *Front. Microbiol.* **9**, 1565 (2018).
39. Y. Zhang, C. A. Gross, Cold shock response in bacteria. *Annu. Rev. Genet.* **55**, 377–400 (2021).
40. M. H. Saier Jr., Families of transmembrane transporters selective for amino acids and their derivatives. *Microbiology* **146**, 1775–1795 (2000).
41. C. Ziegler, E. Bremer, R. Kramer, The BCCT family of carriers: From physiology to crystal structure. *Mol. Microbiol.* **78**, 13–34 (2010).
42. A. R. Curson, J. D. Todd, M. J. Sullivan, A. W. Johnston, Catabolism of dimethylsulphoniopropionate: Microorganisms, enzymes and genes. *Nat. Rev. Microbiol.* **9**, 849–859 (2011).
43. A. Tondervik, A. R. Strom, Membrane topology and mutational analysis of the osmotically activated BetT choline transporter of *Escherichia coli*. *Microbiology* **153**, 803–813 (2007).
44. H. Peter, A. Burkovski, R. Kramer, Isolation, characterization, and expression of the *Corynebacterium glutamicum betP* gene, encoding the transport system for the compatible solute glycine betaine. *J. Bacteriol.* **178**, 5229–5234 (1996).
45. S. Ressl, A. C. Terwisscha van Scheltinga, C. Vonrhein, V. Ott, C. Ziegler, Molecular basis of transport and regulation in the Na^+/betaine symporter BetP. *Nature* **458**, 47–52 (2009).
46. C. Perez, C. Koshy, O. Yildiz, C. Ziegler, Alternating-access mechanism in conformationally asymmetric trimers of the betaine transporter BetP. *Nature* **490**, 126–130 (2012).
47. C. Perez, B. Faust, A. R. Mehdipour, K. A. Francesconi, L. R. Forrest, C. Ziegler, Substrate-bound outward-open state of the betaine transporter BetP provides insights into Na^+ coupling. *Nat. Commun.* **5**, 4231 (2014).
48. S. Schulze, S. Koster, U. Geldmacher, A. C. Terwisscha van Scheltinga, W. Kühlbrandt, Structural basis of Na^+-independent and cooperative substrate/product antiport in CaiT. *Nature* **467**, 233–236 (2010).
49. L. Tang, L. Bai, W. H. Wang, T. Jiang, Crystal structure of the carnitine transporter and insights into the antiport mechanism. *Nat. Struct. Mol. Biol.* **17**, 492–496 (2010).
50. S. Kalayil, S. Schulze, W. Kühlbrandt, Arginine oscillation explains Na^+ independence in the substrate/product antiporter CaiT. *Proc. Natl. Acad. Sci. U.S.A.* **110**, 17296–17301 (2013).
51. M. Haardt, B. Kempf, E. Faatz, E. Bremer, The osmoprotectant proline betaine is a major substrate for the binding-protein-dependent transport system ProU of *Escherichia coli* K-12. *Mol. Gen. Genet.* **246**, 783–796 (1995).
52. C. Oswald, S. H. Smits, M. Höing, L. Sohn-Bösser, L. Dupont, D. le Rudulier, L. Schmitt, E. Bremer, Crystal structures of the choline/acetylcholine substrate-binding protein ChoX from *Sinorhizobium meliloti* in the liganded and unliganded-closed states. *J. Biol. Chem.* **283**, 32848–32859 (2008).
53. N. Barland, A. S. Rueff, G. Cebrero, C. A. J. Hutter, M. A. Seeger, J. W. Veening, C. Perez, Mechanistic basis of choline import involved in teichoic acids and lipopolysaccharide modification. *Sci. Adv.* **8**, eabm1122 (2022).
54. S. H. Smits, M. Höing, J. Lecher, M. Jebbar, L. Schmitt, E. Bremer, The compatible-solute-binding protein OpuAC from *Bacillus subtilis*: Ligand binding, site-directed mutagenesis, and crystallographic studies. *J. Bacteriol.* **190**, 5663–5671 (2008).
55. C. Perez, C. Koshy, S. Ressl, S. Nicklisch, R. Kramer, C. Ziegler, Substrate specificity and ion coupling in the Na^+/betaine symporter BetP. *EMBO J.* **30**, 1221–1229 (2011).
56. C. J. Tsai, K. Khafizov, J. Hakulinen, L. R. Forrest, L. R. Forrest, R. Kramer, W. Kühlbrandt, C. Ziegler, Structural asymmetry in a trimeric Na^+/betaine symporter, BetP, from Corynebacterium glutamicum. *J. Mol. Biol.* **407**, 368–381 (2011).
57. C. Perez, K. Khafizov, L. R. Forrest, R. Kramer, C. Ziegler, The role of trimerization in the osmoregulated betaine transporter BetP. *EMBO Rep.* **12**, 804–810 (2011).
58. Y. Xie, S. Chang, C. Zhao, F. Wang, S. Liu, J. Wang, E. Delpire, S. Ye, J. Guo, Structures and an activation mechanism of human potassium-chloride cotransporters. *Sci. Adv.* **6**, eabc5883 (2020).
59. Y. Dong, H. Li, A. Ilie, Y. Gao, A. Boucher, X. C. Zhang, J. Orlowski, Y. Zhao, Structural basis of autoinhibition of the human NHE3-CHP1 complex. *Sci. Adv.* **8**, eabn3925 (2022).
60. Y. Wang, C. Pan, Q. Chen, Q. Xie, Y. Gao, L. He, Y. Li, Y. Dong, X. Jiang, Y. Zhao, Architecture and autoinhibitory mechanism of the plasma membrane Na^+/H^+ antiporter SOS1 in *Arabidopsis*. *Nat. Commun.* **14**, 4487 (2023).
61. Y. Zhang, J. Zhou, X. Ni, Q. Wang, Y. Jia, X. Xu, H. Wu, P. Fu, H. Wen, Y. Guo, G. Yang, Structural basis for the activity regulation of Salt Overly Sensitive 1 in *Arabidopsis* salt tolerance. *Nat. Plants* **9**, 1915–1923 (2023).
62. X. Y. Zhang, L. H. Tang, J. W. Nie, C. R. Zhang, X. Han, Q. Y. Li, L. Qin, M. H. Wang, X. Huang, F. Yu, M. Su, Y. Wang, R. M. Xu, Y. Guo, Q. Xie, Y. H. Chen, Structure and activation mechanism of the rice Salt Overly Sensitive 1 (SOS1) Na^+/H^+ antiporter. *Nat. Plants* **9**, 1924–1936 (2023).
63. A. Punjani, J. L. Rubinstein, D. J. Fleet, M. A. Brubaker, cryoSPARC: Algorithms for rapid unsupervised cryo-EM structure determination. *Nat. Methods* **14**, 290–296 (2017).
64. J. Zivanov, T. Nakane, B. O. Forsberg, D. Kimanius, W. J. Hagen, E. Lindahl, S. H. Scheres, New tools for automated high-resolution cryo-EM structure determination in RELION-3. *eLife* **7**, e42166 (2018).
65. S. Q. Zheng, E. Palovcak, J. P. Armache, K. A. Verba, Y. Cheng, D. A. Agard, MotionCor2: Anisotropic correction of beam-induced motion for improved cryo-electron microscopy. *Nat. Methods* **14**, 331–332 (2017).
66. K. Zhang, Gctf: Real-time CTF determination and correction. *J. Struct. Biol.* **193**, 1–12 (2016).
67. J. Zivanov, T. Nakane, S. H. W. Scheres, A Bayesian approach to beam-induced motion correction in cryo-EM single-particle analysis. *IUCrJ* **6**, 5–17 (2019).

68. R. Sanchez-Garcia, J. Gomez-Blanco, A. Cuervo, J. M. Carazo, C. O. S. Sorzano, J. Vargas, DeepEMhancer: A deep learning solution for cryo-EM volume post-processing. *Commun. Biol.* **4**, 874 (2021).
69. J. Jumper, R. Evans, A. Pritzel, T. Green, M. Figurnov, O. Ronneberger, K. Tunyasuvunakool, R. Bates, A. Zidek, A. Potapenko, A. Bridgland, C. Meyer, S. A. A. Kohl, A. J. Ballard, A. Cowie, B. Romera-Paredes, S. Nikolov, R. Jain, J. Adler, T. Back, S. Petersen, D. Reiman, E. Clancy, M. Zielinski, M. Steinegger, M. Pacholska, T. Berghammer, S. Bodenstein, D. Silver, O. Vinyals, A. W. Senior, K. Kavukcuoglu, P. Kohli, D. Hassabis, Highly accurate protein structure prediction with AlphaFold. *Nature* **596**, 583–589 (2021).
70. P. Emsley, B. Lohkamp, W. G. Scott, K. Cowtan, Features and development of *Coot*. *Acta Crystallogr. D Biol. Crystallogr.* **66**, 486–501 (2010).
71. P. D. Adams, P. V. Afonine, G. Bunkoczi, V. B. Chen, I. W. Davis, N. Echols, J. J. Headd, L. W. Hung, G. J. Kapral, R. W. Grosse-Kunstleve, A. J. McCoy, N. W. Moriarty, R. Oeffner, R. J. Read, D. C. Richardson, J. S. Richardson, T. C. Terwilliger, P. H. Zwart, PHENIX: A comprehensive Python-based system for macromolecular structure solution. *Acta Crystallogr. D Biol. Crystallogr.* **66**, 213–221 (2010).
72. V. B. Chen, W. B. Arendall III, J. J. Headd, D. A. Keedy, R. M. Immormino, G. J. Kapral, L. W. Murray, J. S. Richardson, D. C. Richardson, MolProbity: All-atom structure validation for macromolecular crystallography. *Acta Crystallogr. D Biol. Crystallogr.* **66**, 12–21 (2010).
73. The PyMOL Molecular Graphics System, Version 2.0 (Schrödinger LLC, 2017).
74. E. F. Pettersen, T. D. Goddard, C. C. Huang, G. S. Couch, D. M. Greenblatt, E. C. Meng, T. E. Ferrin, UCSF Chimera—A visualization system for exploratory research and analysis. *J. Comput. Chem.* **25**, 1605–1612 (2004).
75. E. F. Pettersen, T. D. Goddard, C. C. Huang, E. C. Meng, G. S. Couch, T. I. Croll, J. H. Morris, T. E. Ferrin, UCSF ChimeraX: Structure visualization for researchers, educators, and developers. *Protein Sci.* **30**, 70–82 (2021).

Acknowledgments: We thank D. Li and X. Li at the Core Facility of Wuhan University for help with cryo-EM data collection. We thank the State Key Laboratory of Genetic Engineering Cryo-EM Facility of Fudan University for sample imaging. **Funding:** This work was made possible by support from the CAS Center for Excellence in Molecular Plant Sciences, the CAS Pioneer Hundred Talents Program, and the Strategic Priority Research Program of Chinese Academy of Sciences (XDB0630101) to M.F. J.Z. was supported by startup funding from Fudan University. G.A.B. was supported by the USDA National Institute of Food and Agriculture, Hatch project IOW04308. **Author contributions:** T.Y., Y.N., H.L., and J.L. performed most of the research and equally contributed to this work. Conceptualization: M.F., J.Z., G.A.B., T.Y., Y.N., and H.L. Investigation: T.Y., Y.N., H.L., J.L., J.Z., and M.F. Methodology: T.Y., Y.N., H.L., X.L., J.Z., and M.F. Visualization: T.Y., Y.N., H.L., X.L., G.A.B., J.Z., and M.F. Validation: T.Y., Y.N., H.L., T.L., R.W., J.Z., and M.F. Formal analysis: T.Y., Y.N., H.L., X.L., J.Z., and M.F. Data curation: T.Y., Y.N., H.L., J.Z., and M.F. Software: X.L. and J.Z. Resources: M.F., J.Z., G.A.B., L.W., and X.L. Supervision: M.F. and L.W. Project administration: M.F., J.Z., and L.W. Funding acquisition: M.F. Writing—original draft: M.F., J.Z., G.A.B., T.Y., Y.N., H.L., and J.L. with input from all coauthors. Writing—review and editing: M.F., J.Z., T.Y., Y.N., and H.L. with input from all coauthors. **Competing interests:** The authors declare that they have no competing interests. **Data and materials availability:** All data needed to evaluate the conclusions in the paper are present in the paper and/or the Supplementary Materials. The cryo-EM maps of PsBetT are available in the Electron Microscopy Data Bank under EMD-39121 and EMD-39122. The corresponding models are available in the Protein Data Bank under 8YBQ and 8YBR.

Submitted 12 February 2024
Accepted 9 July 2024
Published 14 August 2024
10.1126/sciadv.ado6229